

Evaluation of the Effective Flange Width of Mass Timber Composites Beams Using Digital Image Correlation and Finite Element Modelling

Tyler Hull¹, Daniel Lacroix²

ABSTRACT: Shear lag in the flanges of mass timber composite panels can result in inaccurate estimations of the bending stresses and deflections of these elements. The effective flange width (EFW), used to account for shear lag in design, is evaluated on 4.5m cross-laminated timber flange and glulam web T-beams, joined using screw-gluing, using digital image correlation (DIC), finite element modelling (FEM), and discrete strain gauges. DIC proved to be a valuable measurement technique for capturing a large field of strains and minimized the strain peaks and valleys due to local wood characteristics which can impact discrete strain gauge outputs. DIC strain distributions showed good agreement with FEM results. The EFW determined using DIC was on average 88-89% for midspan loading compared to 93-94% using the FEM. Edge-gluing behaviour was not captured in current FEM techniques and could be responsible for the difference in results. Experimental and FEM EFW results are compared to the proposed Eurocode 5 equations for estimating the EFW in design. A modified method for evaluating the full-depth EFW of multi-layer CLT panels is also proposed for cases where tensile strain can develop in lower layers and rolling shear can occur in the perpendicular layers.

KEYWORDS: Mass timber composite, Ribbed panel, Digital image correlation, Effective flange width, CLT

1 – INTRODUCTION

Achieving long-span floors is frequently required for industrial, commercial, institutional, and residential building types to adapt to the functional needs of the desired layout. In mass timber buildings, a viable floor system for spans up to 16m is compositely connecting the slabs and beams to form ribbed or hollow core panels, commonly referred to as mass timber composites (MTCs). MTCs often consist of cross-laminated timber (CLT) slabs and glulam beams compositely connected with a shear connection consisting of adhesive, mechanical fasteners, or a combination thereof (Fig. 1).

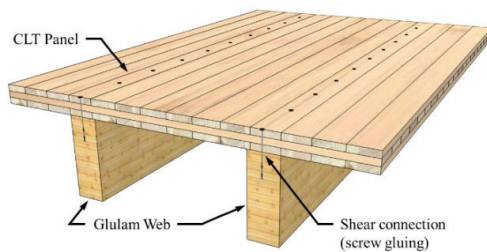


Figure 1. Mass timber composite ribbed panel

The large spacing between the beams impacts the behaviour of in-plane shear stress in the flange, with the

longitudinal strains over the voided spaces lagging those close to the beams. This phenomenon, termed “shear lag”, leads to a non-uniform distribution of longitudinal strains across the width of the flange and can result in inaccurate estimations of stresses and deflections based on classical Euler-Bernoulli beam theory [1]. In practice, the concept of the effective flange width (EFW) has been introduced for other materials to account for this phenomenon and allow Euler-Bernoulli beam theory to be applied. However, guidance for the EFW in mass timber elements is limited and generally lacking in current design codes in Canada and internationally.

This paper, as part of a larger study on MTC panels, evaluates the strain distribution across the top of the flange of three 4.5m CLT-glulam T-beams that are compositely connected with a screw-glued (SG) shear connection at service level testing caused by two different loading profiles. The longitudinal strains obtained experimentally using digital image correlation (DIC) and discrete strain gauges are presented, and compared to numerical results of a verified finite element model (FEM). Recommendations for utilizing DIC with wood materials are discussed. A modified method for evaluating the full-depth EFW of multi-layer CLT panels is also proposed.

¹ Tyler Hull, B.A.Sc., Department of Civil and Environmental Engineering, University of Waterloo, Waterloo, Canada, tyler.hull@uwaterloo.ca

² Daniel Lacroix, Ph.D., Department of Civil and Environmental Engineering, University of Waterloo, Waterloo, Canada, daniel.lacroix@uwaterloo.ca

2 – BACKGROUND

2.1 EFFECTIVE WIDTH OF WOOD-WOOD COMPOSITES

The effective width defines an equivalent cross-section such that the maximum bending stress and effective bending stiffness remain the same as the actual cross-section when applying simple beam formula [1]. This method is advantageous for its simplicity and allows for the use of simple beam theory in design. Historically, for wood structural elements, guidance for the EFW in the CSA O86: *Engineering design in wood* standard [2] has been limited to stressed-skinned panels where plywood panels are fastened to the top and bottom of sawn lumber web members. Shear lag is accounted for in these elements by a geometry modification factor (i.e., EFW) that is dependent on the web/rib clear spacing and panel span [3].

Thicker flanges were considered in further studies on stress-laminated T-systems for timber bridges when vertically laminated timber decks are post-tensioned transversely by high-strength steel bars. Davalos and Salim [4] proposed an equation for the EFW which depended on the stringer-to-web spacing, bridge span, ratio of stringer depth to deck thickness, and ratio of longitudinal stringer elastic modulus to deck elastic modulus. Apple and Woodward [5] investigated a similar system but with steel wide flange section webs rather than glulam. A series of T-beams were investigated numerically with three different deck thicknesses and three beam spacings. The results showed EFWs varying between 0.79 - 0.86 times that of the beam spacing.

With the increasing uptake of mass timber products in recent years, a handful of studies have considered thicker CLT flanges. Bogensperger [6] analyzed CLT-glulam T-beams using a beam and in-plane loaded plate connected by a spring. A proposed relationship based on the type of loading, level of loading (ULS vs. SLS), single vs. multi-span beam, and stiffness and shear flexibility of the CLT element was developed. It was also noted the EFW varied on the length of the T-beam, with the maximum occurring in the middle of the span and declining in the direction of the supports. Thiel et al. [7] followed this work by proposing an EFW for determining the maximum rolling shear stress which was equal to the width of the rib plus a 45° dispersion angle through the first layer if it ran parallel to the span. Masoudnia et al. [8] experimentally evaluated the EFW of laminated veneer lumber-CLT T-beams that were instrumented with several displacement gauges across the width at midspan. The experimental result agreed well with the *ABAQUS* [9] FEM in terms of EFW, midspan deflection, and slip between elements. The FEM was used to conduct a parametric analysis which found that additional parameters including transverse layer thickness, wood plank widths within the CLT, modulus of elasticity of the transverse layers, and shear connection stiffness impacted the EFW. Hull and Lacroix [10] found a similar

group of influential parameters in their numerical study of glued-laminated timber (GLT) panels and glulam beam MTCs (i.e., I-beams), noting that the most significant parameters as web spacing, shear connection stiffness, loading type, flange thickness, and web width.

In the final draft for the revised version of Eurocode 5 [11], the design standard for timber structures, simplified equations for estimating the EFW for CLT ribbed panels are proposed based on the previous literature and a report by Augustin and Thiel [12]. Equation (1) defines the effective width from Eurocode 5 [11], $b_{ef,EC5}$:

$$b_{ef,EC5} = \min \left\{ b_w + \sum_b b_{ef,i} \right. \quad (1)$$

where b_w is the width of the web, $b_{ef,i}$ is the effective width each side of the web defined in (2) for midspan point loading, and b is the centre-to-centre spacing between webs.

$$b_{ef,i} = b_{f,i} \left(0.5 - 0.30 \left(\frac{b_{f,i}}{L} \right)^{0.25} \left(\frac{(EA)_x}{S^*_{xy}} \right)^{0.25} \right) \quad (2)$$

Where, $b_{f,i}$ is the clear distance between webs, L is the span, $(EA)_x$ is the in-plane stiffness of the CLT panel in the span direction (i.e., $E_{i,0,mean}$ x the area, A , of each layer), and S^*_{xy} is the in-plane shear stiffness of the CLT from Eurocode 5 [13]. Kleinhenz et al [14] compared their experimental results for the EFW of 12 CLT-glulam T- and I-beams to the results of the proposed equation for uniformly distributed loading. Overall, the average EFW was determined to be 80% based on the experimental results and 60% as estimated by the proposed equations.

2.2 EFFECTIVE WIDTH DETERMINATION

In its general form, the effective width, b_{eff} , can be related to the non-uniform stress distribution in the flange by (3):

$$\sigma_{x,max}(z) \cdot b_{eff} = \int \sigma_x(y,z) d_y \quad (3)$$

where, $\sigma_{x,max}(z)$ is the maximum longitudinal bending stress distribution along the thickness of the flange at the rib centre, and $\int \sigma_x(y,z) d_y$ is the integral of the longitudinal bending stress along the thickness and width of the flange [14]. In principle, the EFW maintains the maximum bending stress in the extremity of the flange by reducing the width of the flange. This concept is demonstrated for a CLT-glulam T-beam in Fig. 2.

Chiewanichakorn et al. [15] proposed a method for evaluating the EFW from FEM results for single-layer thick flanges where the neutral axis can migrate into the flange. This method is presented in (4):

$$b_{eff} = \frac{C_{slab}}{F} = \frac{C_{slab}}{0.5 \cdot t_{slab} \cdot (\sigma_{max} + \sigma_{min})} \quad (4)$$

where, C_{slab} is the total compression force in the slab from the FEM, F is the magnitude of the equivalent trapezoidal shape per unit width, t_{slab} is the thickness of the flange,

σ_{max} and σ_{min} are the maximum and minimum axial stresses from the trapezoidal stress profile, respectively. In this definition, two assumptions are made and held throughout the calculation: 1) bending moments computed from the FEM are the same as from simple beam theory, and 2) the equilibrium of section forces and moment is always maintained. To satisfy both assumptions, the magnitude of the longitudinal force in the flange and its centroidal location, z_0 , must be the same for both the FEM and simple beam theory [15]. To enforce the centroidal location criteria, the FEM centroid location from the slab top edge, $z_{0,FEM}$ defined by (5), must be equal to the centroid location from simple beam theory, $z_{0,eff}$. This relationship is solved by holding the maximum stress value, σ_{max} , equal to the maximum value from the FEM and varying σ_{min} until z_0 from both calculations are equal.

$$z_{FEM} = \frac{M_{slab}}{C_{slab}} \quad (5)$$

Where M_{slab} is the total bending moment contributed by the slab about the top edge and is defined by (6).

$$M_{slab} = \sum_{i=1}^n C_{i,slab} \cdot z_i = \sum_{i=1}^n \sigma_i \cdot A_i \cdot z_i \quad (6)$$

Where n is the total number of subdivided slab elements across the width, i is the slab element number, σ_i is the average longitudinal stress of the slab element, A_i is the slab element cross-sectional area, and z_i is the distance from the slab element centroid to the top edge of the slab. Once σ_{min} is determined using this method, the EFW can be calculated using (4).

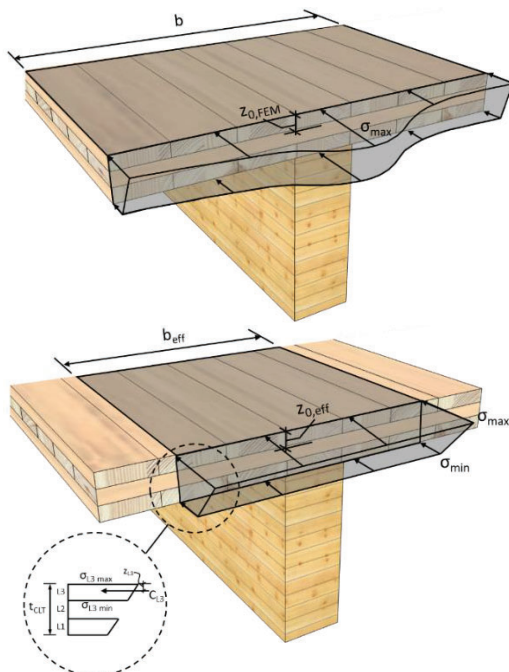


Figure 2. EFW of CLT-glulam T-beam, (top) non-uniform distribution, (bottom) trapezoidal effective distribution

3 – EXPERIMENTAL TESTING

3.1 TEST CONFIGURATIONS

The CLT-glulam T-beams consisted of an 80mm x 245mm SPF 20f-EX glulam beam and 105mm deep x 1m wide V2 grade edge-glued CLT slab compositely connected using a SG shear connection comprised of 8mm diameter x 240mm long TBS washer head screws plus an additional 26.0mm diameter washer. Screws were spaced at 300mm and two 9mm wide beads of PL Premium Max construction adhesive were used [16]. The configuration is shown in Fig. 3.

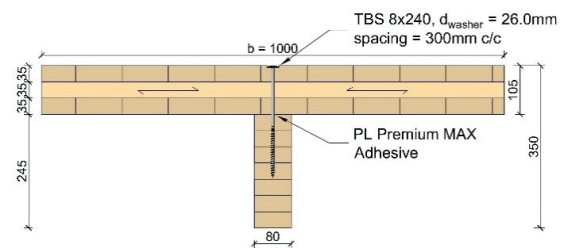


Figure 3. Screw-glued (SG) T-beam configurations

3.2 TEST SETUP AND PROCEDURE

3.2.1 Non-destructive evaluation of elements

To predict the behaviour of the T-beam specimens in the FEM and material models, the modulus of elasticity (MOE) of the webs and flanges is required. These were determined individually for each web and flange element through non-destructive stress testing prior to their assembly into the T-beam specimens. Both elements were loaded in four-point bending according to ASTM D198-22a: *Standard Test Methods of Static Tests of Lumber Sizes* [17] with an a/d ratio greater than 6, which is recommended when evaluating primarily for deflection. A linear variable displacement transducer (LVDT) was installed at midspan to measure the deflection. CLT and glulam elements were loaded to approximately 15% maximum load until a representative linear load-displacement curve was achieved. Both elements were tested at a loading rate of 3mm/min, which resulted in a time to specified load of 2-3min. The stress test setup is shown in Fig. 4. Since the displacements recorded during testing included deformations due to shear, the MOE determined using classical beam theory resulted in the apparent modulus of elasticity, E_{app} . The shear-free MOE, E_{sf} , was determined for the two-point loading scenario according to (7) from Table X2.1 of ASTM D198-22a [17] by removing the shear deformations from the midspan deflection, Δ_{mid} , data.

$$E_{sf} = \frac{\frac{F}{2} a(3L^2 - 4a^2)}{4bd^3\Delta \left(1 - \frac{3 \cdot F/2 \cdot a}{5bdG\Delta_{mid}}\right)} \quad (7)$$

Where F is the actuator load, L is the clear span of the specimen (4.2m), a is the distance from the load point to the support (1500mm for glulam, 1400mm for CLT), b is

the width, d is the depth, and G is the shear modulus. G is taken as $E_{app}/16$ for the glulam webs based on recommendations from CSA O86 [2]. For the CLT panels, I and GA were taken from CSA O86 [2] and used to determine E_{app} and E_{sf} .



Figure 4. MOE determination test setup

3.2.2 T-beam evaluation

The test setup had a clear span of 4.2m with loading applied as a discrete point load in the middle of the panel and as a line load across the width of the CLT at midspan. During testing, the applied load was measured using the load cell in the hydraulic frame, and the displacement at midspan was measured using a string potentiometer installed, near the estimated neutral axis, at 215mm from the bottom. Three strain gauges were placed across the top surface of the CLT to measure the non-uniform compressive strain, along with one on the bottom of the glulam web to measure the maximum tensile strain. Fig. 5 summarizes the experimental test setup.

In addition to the conventional strain gauges, a 3D digital image correlation (DIC) system was also installed in an overhead fashion to capture the top surface strain field. DIC is a non-contact, optical method to capture 3D

deformations on the surface of an object based on relative changes in sequential images [18]. Two 5MP cameras with 8mm lens simultaneously captured images of a 1000mm x 1000mm speckle pattern area directly adjacent to the loading point. Due to the loading being applied at midspan, the compression strains on the top surface were evaluated for the DIC, FEM, and strain gauges at a distance 450mm from the midspan of the panel. Cameras were mounted on a separate support arm from the hydraulic test frame at approximately 1.2m from the CLT and an angle of 16° between cameras. A 5.08mm random black speckle using the manufacturer provided roller was applied in 3 layers at angles 0, 90, and 45 degrees on a matte white paint undercoat. A high contrast pattern improves analysis accuracy [18]. Initial zero-displacement images were analyzed to verify the system calibration using specimens' dimensions and distance between the cameras.

The loading was applied at set actuator displacement increments of 0, 2, 4, 6 and 8mm, where at each level of displacement, the test was briefly paused and 20 DIC images per camera were taken for analysis once the hydraulics stabilized. Images were captured using the manual capture feature of VIC-Snap 9. Images were captured in groups of 20 at each set interval so that they could later be averaged using the "time average" function of Vic-3D. Initially, images were captured continuously at a rate of 2Hz. However, due to the lower levels of strain ($< 500\mu\epsilon$) at this loading, small amounts of noise in the area of interest (approximately $50\mu\epsilon$) could influence the analysis results. Small amounts of noise are generally unavoidable even for ideal test setups [19]. The time average method was used to minimize the noise in the results by averaging the readings across the 20 images. A subset size of 39 pixels was used for the DIC analysis. The software VIC 3D Digital Image Correlation Version 10.0.8 [20] was used for calibration and analysis.

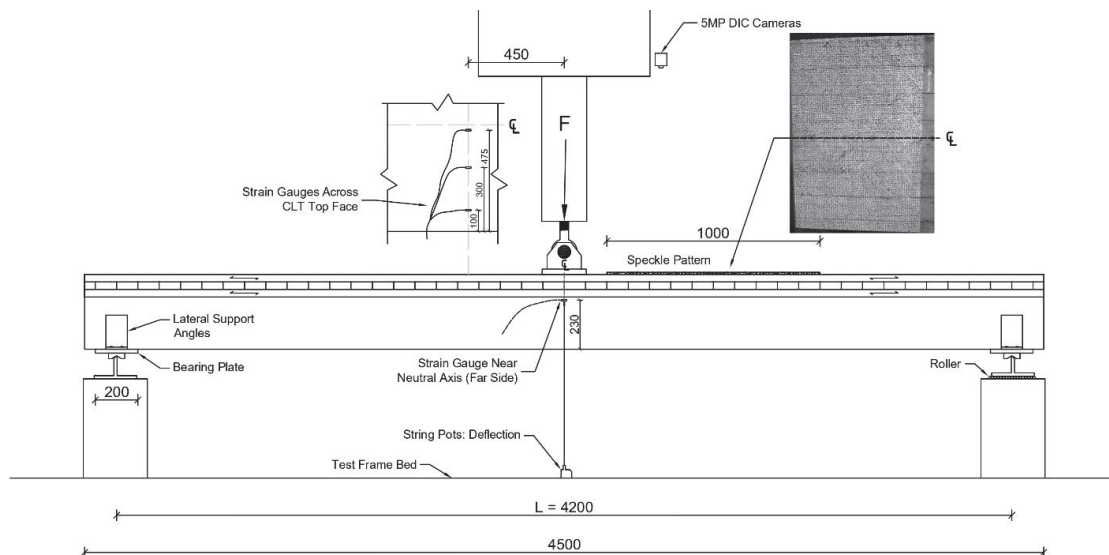


Figure 5. T-beam bending test setup

4 – NUMERICAL ANALYSIS

The numerical model was developed in Abaqus CAE finite element software [9]. The CLT and glulam were modelled as separately defined elements with a contact interaction between them. The 200mm wide bearing plate was also added as a roller support and modelled as a 3D discrete rigid shell to limit local crushing. The two loading conditions, point load (200mm x 200mm) and line load (200mm x 1000mm) are modelled as 3D rigid shell elements with an equivalent pressure load applied equal to the experimental test load divided over the contact area. A vertical geometric symmetry simplification was defined along the midspan and cross-section centreline such that only ¼ of the model need be modelled (Fig. 6). The contact between the web and flange was modelled as a cohesive contact in the sliding direction and a “hard” contact in the normal direction. The stiffness of the cohesive bond, K_{ss} , was used to simulate the stiffness of the shear connection per unit length and was taken as the initial linear stiffness, $k_{s,0.1-0.4}$ from [21]. Contact between the composite element and the fixed support blocks was modelled as a “hard” contact in the normal direction and a frictional penalty coefficient of 0.05 in the tangential direction. The wood elements were modelled as a linear-elastic orthotropic material using ABAQUS’ engineering constants option, where the primary spanning direction (1) represents the longitudinal direction of the wood grain and the two secondary directions (2) and (3) represent the two perpendicular to grain directions. For the CLT specifically, the 3D solid element was partitioned into three layers of equal thickness, and the orientation of the middle layer was modified such that the primary direction (E_1) ran in the width direction of the panel (i.e., perpendicular to the span) to represent the cross-layer. A mesh of 12.5mm x 12.5mm was used for the CLT flange with 3 elements explicitly specified for the height of each layer. A 20mm x 20mm mesh was used for the glulam web. The loading block used a 12.5mm x 12.5mm mesh while the support block used a 40mm x 40mm mesh.

The material properties used for the wood elements are presented in Table 1. The moduli of elasticity values were taken from the experimental testing, whereas the Poisson’s ratios were obtained from average values from Bartolucci et al. [22] for similar species to the white and black spruce commonly used by the manufacturer.

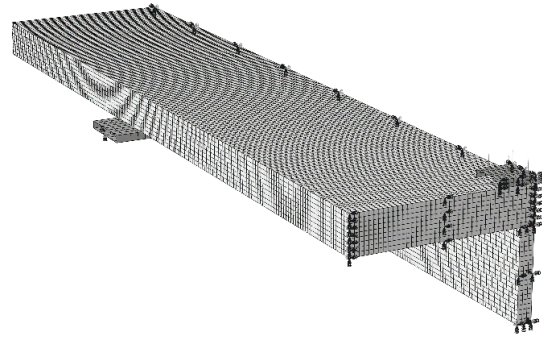


Figure 6. Point load finite element model

5 – RESULTS

5.1 MOE DETERMINATION

The results of the MOE determination for the CLT and glulam elements are presented in Table 2. Overall, the glulam webs had an average E_{sf} of 13,118MPa with a CoV of 0.03, while the CLT flanges had an average E_{sf} of 10,724MPa with a CoV of 0.06. The average moisture content immediately after testing was 12.9% for the glulam and 11.9% for the CLT, with all readings within 11.1% and 13.6%.

Table 2. Modulus of elasticity results

	Glulam		CLT	
	E_{app}	E_{sf}	E_{app}	E_{sf}
SG-01	12,738	13,443	9,156	9,906
SG-02	12,553	13,249	10,327	11,291
SG-03	11,997	12,662	10,062	10,975
Avg.	12,429	13,118	9,848	10,724
CoV	0.03	0.03	0.05	0.06

5.2 FEM VALIDATION

To validate the FEM the midspan deflection, Δ_{mid} , and maximum tensile strain at the bottom of the glulam web, $\epsilon_{bot,mid}$, were requested from the final 8mm load step. The parameters are compared between the experimental results and FEM in Fig. 7 and Fig. 8. The results for the midspan deflection showed good correlation with an R^2 value of 0.80. The maximum tensile strain results showed a lower correlation with an R^2 value of 0.05.

Table 1. Material properties for CLT and glulam in FEM

Element	E_1	E_2	E_3	$\nu_{12}^{(b)}$	$\nu_{12}^{(b)}$	$\nu_{12}^{(b)}$	G_{12}	G_{13}	G_{23}
	[N/mm ²]	[N/mm ²]	[N/mm ²]	[-]	[-]	[-]	[N/mm ²]	[N/mm ²]	[N/mm ²]
CLT _{L1,L3}	$E_{sf}^{(a)}$	$E_{sf}/30$	$E_{sf}/30$	0.40	0.40	0.37	$E_{sf}/16$	$E_{sf}/16$	$G_{12}/10$
CLT _{L2}	9000 ^(c)	300	300	0.40	0.40	0.37	562.5	562.5	56.3
Glulam	$E_{sf}^{(a)}$	$E_{sf}/30$	$E_{sf}/30$	0.40	0.40	0.37	$E_{sf}/16$	$E_{sf}/16$	$G_{12}/10$

^(a) E_{sf} provided in Table #

^(b) Values based on Bartolucci et al. [22]

^(c) Values based on transverse layer of V2 grade CLT from CSA O86 [2]

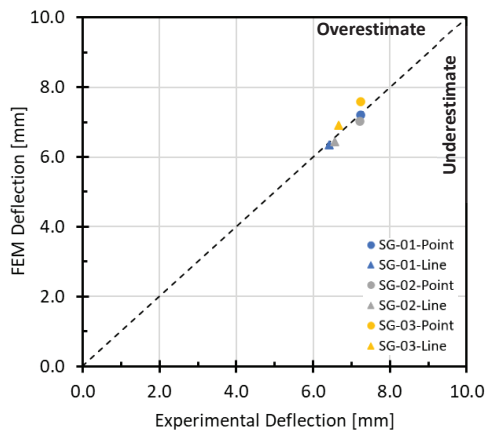


Figure 7. Midspan deflections – experimental results by LVDT compared to FEM results

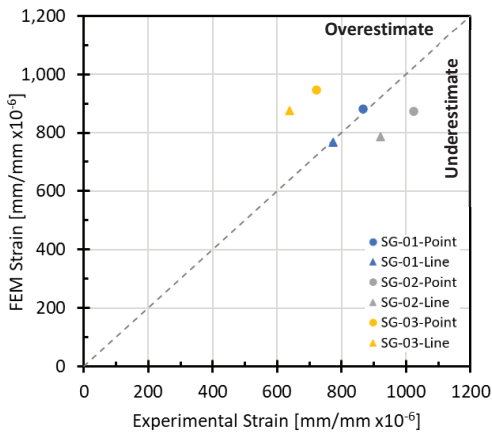


Figure 8. Maximum tensile strain – experimental results by strain gauge compared to FEM results

5.3 TOP SURFACE STRAIN DISTRIBUTION

The results of the strain distribution across the top surface of the CLT flange were compared for the DIC, FEM, and strain gauge results at a distance 450mm from the midspan of the panel and a load level representative of the final 8mm step. For the DIC results, some “hot spots” were observed in the analysis which were attributed to the natural growth characteristics of wood such as knots and grain deviations, as well as around the screw heads. Fig. 9 shows a representation strain field from the DIC analysis and demonstrates many of the high and low spots occurring near imperfections (e.g., knots) and the screw heads. To reduce the impact of these irregularities on the EFW calculation, the strain results were averaged over nine cut lines over a gauge length of 260mm along the length of the slab. The strain profile was then plotted using 200 extraction points across the width of the CLT panel at each cut line. For the FEM, the strain profile was extracted from a section taken 450mm from the midspan of the model at the CLT flange top surface. Both the DIC and FEM strain profile, along with the discrete strain gauge results are plotted for each specimen in Fig. 10.

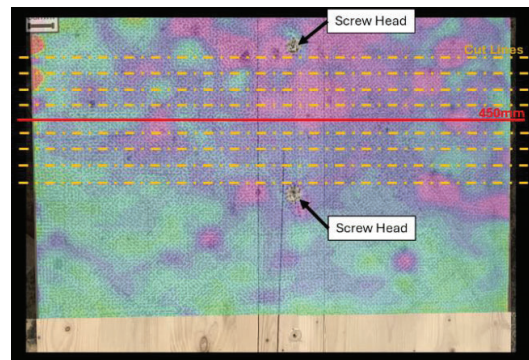


Figure 10. DIC strain field result and cut lines (SG-01-Point)

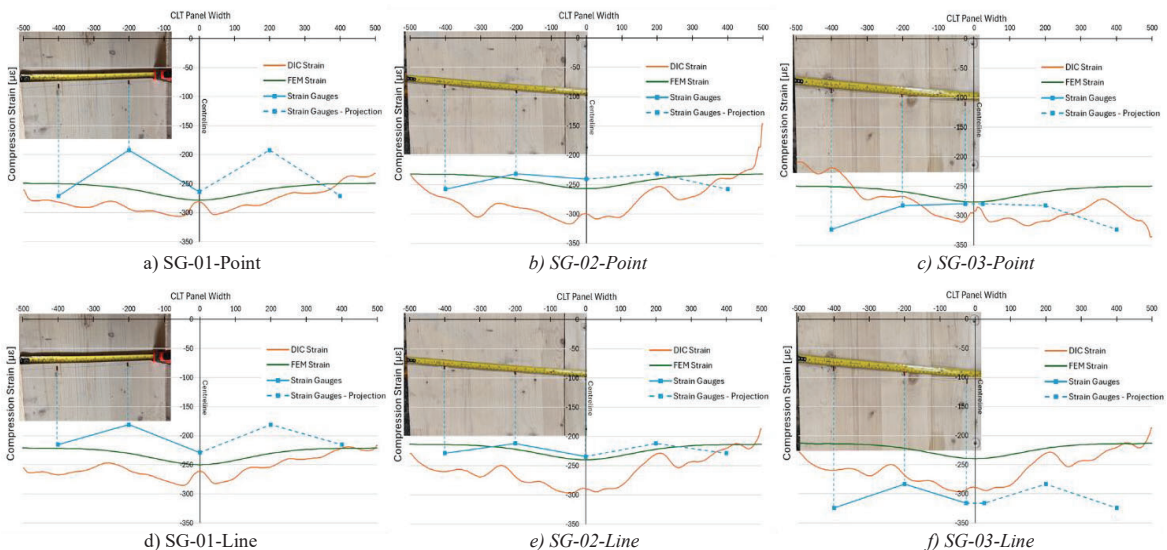


Figure 9. CLT top edge strain distribution – DIC, FEM, strain gauges and strain gauge surface location, a-c) point loading (L-R) SG-01, SG-02, SG-03, d-f) line loading (L-R) SG-01, SG-02, SG-03

The EFW was analyzed using (2) for the top surface of the CLT using the DIC and FEM results. Results for the top surface EFW are presented in Table 3. For the DIC results, the effective width of the top surface of the CLT was on average 89% for the point load (CoV = 0.02) and 88% for the line load (CoV = 0.01). For the FEM results, the effective width of the top surface of the CLT was on average 94% for the point load (CoV = 0.00) and 93% for the line load (CoV = 0.00).

5.4 EFW BASED ON INDIVIDUAL LAYERS

The EFW for each individual layer was analyzed using the method proposed by Chiewanichakorn et al. [15] in (4) to (6), and the FEM results for the top and bottom edge of each longitudinal layer. Since wood is linear elastic for service level strains, strain data for the experimental testing is directly substituted for stress in (3) to (6). Results for the individual layer EFW are presented in Table 3. On average the EFW for the top layer (layer 3) was 94% for the point load and 93% for the line load, while for the layer closest to the shear connection (layer 1) the average EFW was smaller at 30% for the point load and 27% for the line load. It is important to note this method assumes any tension stress/strain in the flange is zero when determining the EFW since it was originally developed for concrete flanges. Layer 1 often developed tension strains near the extremities of the flange in the FEM which were neglected by this method.

5.5 FULL EFFECTIVE FLANGE WIDTH

5.5.1 Proposed Effective Width Definition for CLT

The FEM results were further used to analyze the EFW of the full depth of the CLT flange, which included parallel to grain layer 1 closest to the shear connection, and layer 3 at the top surface. Perpendicular layer 2 is assumed to have zero longitudinal strain and is neglected from the EFW calculation. Given that the method proposed by Chiewanichakorn et al. [15] was derived for a single flange layer, a modified approach is proposed to analyze the full-depth EFW across multiple layers. Similar to the original method, non-uniform results across each layer are integrated to determine the resultant, $\epsilon_{Lj,FEM}$, and lever arm, $z_{Lj,FEM}$, from the top edge of the CLT. The concepts associated with this definition

are shown in Fig. 2. As noted in Section 5.4, since CLT can develop tension strains, rather than being taken as zero strain as per the previous method for a concrete flange [15], any resultant tension strain and its lever arm are calculated as separate from compression strains for each layer. The total resultant strain for all layers, P_{FEM} , and total resultant moment, M_{FEM} , from the FEM are then determined using (8) and (9), respectively.

$$P_{FEM} = \sum_{j=1}^m \epsilon_{Lj} = \sum_{j=1}^m \left\{ \begin{array}{ll} \sum_{i=1}^n \epsilon_{Lj,i} \cdot A_{Lj,i} & j = \text{odd} \\ 0 & j = \text{even} \end{array} \right. \quad (8)$$

$$M_{FEM} = \sum_{j=1}^m \epsilon_{Lj} \cdot z_j \quad (9)$$

Where m is the total number of layers, j is the layer number, ϵ_{Lj} is the tension or compression resultant strain for each layer j , $\epsilon_{Lj,i}$ is the average longitudinal strain of the layer element, A_i is the layer element cross-sectional area, M_{FEM} is the total bending moment contributed by the layer about the top edge, and z_i is the distance from the layer element centroid to the top edge of the CLT.

Since the perpendicular middle layer experiences rolling shear between layers 1 and 3, strain distributions do not coincide between layers. There is a jump in strain between layers due to this, which is shown in Fig. 11 from the SG-01-Point FEM results. This jump can vary across the width of the CLT, growing larger towards the extremities of the flange (Fig. 12). To account for this jump while maintaining ϵ_{max} and ϵ_{min} as the defining variables of the trapezoidal shape, the slope from the top of layer maximum strain to the bottom of layer minimum strain is set to the average slope within each layer from the FEM results. An example of the transformation from FEM distribution over the height of the section to the equivalent trapezoidal-shaped distribution in the CLT is demonstrated in Fig. 11.

Table 3. Effective flange width results based on DIC and FEM strain distribution

Specimen	Type	Load, F [kN]	Top Edge EFW		Layer EFW		Total EFW	
			DIC	FEM	Layer 3	Layer 1	b_{effFEM}/b_{CLT}	b_{effFEM}/b_{CLT}
			[-]	[-]	[-]	[-]	[-]	[-]
SG-01	Point	25.9	0.91	0.93	0.93	0.33	0.92	0.21
	Line	23.0	0.89	0.92	0.92	0.30	0.92	0.21
SG-02	Point	26.0	0.87	0.94	0.94	0.28	0.93	0.21
	Line	23.9	0.87	0.93	0.93	0.26	0.92	0.21
SG-03	Point	27.1	0.89	0.94	0.94	0.28	0.93	0.21
	Line	24.9	0.88	0.93	0.93	0.26	0.92	0.21
Mean	Point	26.3	0.89	0.94	0.94	0.30	0.93	0.21
CoV		0.020	0.020	0.003	0.003	0.082	0.003	0.000
Mean	Line	23.9	0.88	0.93	0.93	0.27	0.92	0.21
CoV		0.019	0.010	0.001	0.002	0.073	0.002	0.000

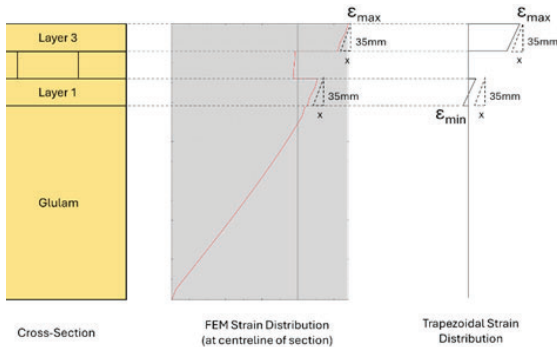


Figure 11. FEM strain distribution (SG-01-Point) over cross-section height at centreline

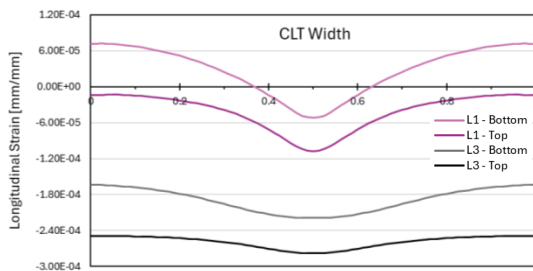


Figure 12. FEM strain distribution (SG-01-Point) across CLT width at top and bottom edge strain of layers 1 and 3

The previous two assumptions of bending moments computed from the FEM being the same as for simple beam theory, and the equilibrium of section forces and moment is always maintained, are set and held throughout the calculation. ϵ_{min} is then changed until $z_{0,FEM}$ is equal to $z_{0,eff}$. Once ϵ_{min} is determined, the effective width, b_{eff} , is determined using (10).

$$b_{eff} = \frac{P_{FEM}}{F_{eff}} \quad (10)$$

Where F_{eff} is the magnitude of the equivalent trapezoidal shape per unit width.

5.5.2 – Full Effective Width Results

The proposed definition from Section 5.5.1 was used to determine the full EFW for each specimen and loading condition. The results of the full EFW calculations are presented in Table 3 along with the proposed Eurocode 5 (EC5) EFW determined using (1) and (2) for a midspan point load. The full-depth effective width of the CLT flange was on average 93% for the point load (CoV = 0.00) and 92% for the line load (CoV = 0.00). The effective flange width from the proposed Eurocode 5 revision, (1), was 21% for all specimens.

6 – DISCUSSION

6.1 – FEM PREDICTIONS

The FEM was able to accurately predict the experimental midspan deflections. However, larger variations were observed between the FEM and the experimental strain

gauge results for the maximum tensile strain on the bottom of the glulam web. For SG-02, the FEM predicted a lower maximum tensile strain than measured by the strain gauge, while for SG-03, the FEM predicted higher strains than the strain gauge. Discrepancies between the two results could be caused by differences in the element material properties or shear connection stiffness, strain readings from discrete gauges being locally impacted by natural growth patterns in the wood (i.e. knots and changes in grain direction), as well as elements adding in manufacturing such as finger joints. It is hypothesized that a finger joint near the strain gauge of SG-02 (Fig. 13), as well as knots and sloped grain near the strain gauge of SG-03 (Fig. 14), impacted the readings of these gauges. Rather than small discrete strain gauges, future projects should consider implementing other strain evaluation methods such as a second DIC for the T-beam elevation, fibre-optic strain sensing cable, or extensometers able to capture wider areas of wood.

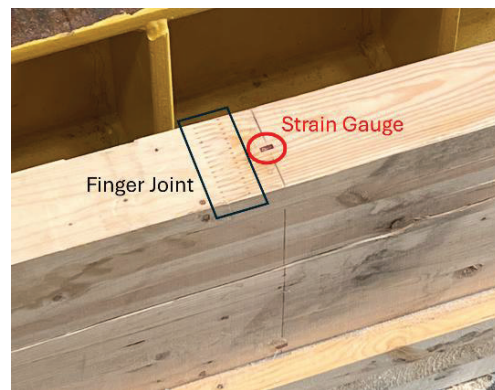


Figure 13. Tensile strain gauge bottom of SG-02 glulam

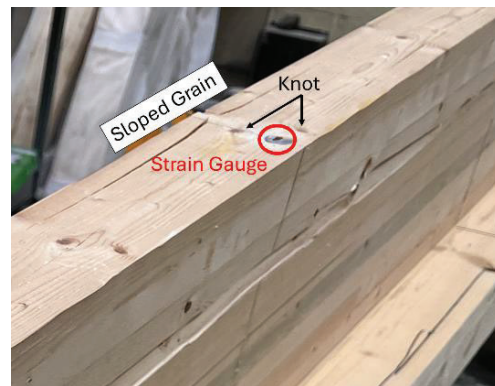


Figure 14. Tensile strain gauge bottom of SG-03 glulam

6.2 – TOP EDGE STRAIN DISTRIBUTION

The strain distributions across the top edge of the CLT flange were compared between the DIC, FEM, and three discrete strain gauges. In general, the DIC and FEM were comparable in terms of shape and decrease from the peak strain over the web to the minimum strain near the extremities of the flange, with the DIC observing more peaks and valleys in the distribution due to the local properties of the wood (see Fig. 10). From Table 3,

similar results for the EFW of the top edge of the CLT for both the DIC and FEM were observed. The 5% difference in effective width between methods was hypothesized to be attributed to the edge-gluing between longitudinal boards and its influence on the shear lag behaviour that was not captured by the FEM. Generally, the DIC tended to overestimate the maximum compression strain by approximately 17% compared to the FEM results (Fig. 10).

Strain gauges across the CLT flange tended to give variable results when compared to the DIC and FEM distributions. Initially, the middle strain gauge was placed directly on the beam centreline (SG-01, SG-02). However, this resulted in the furthest strain gauge from the centreline often exceeding the centreline gauge. This was believed to be due to the large countersunk washers from the screw gluing process impacting the longitudinal strains in this area. Thus, for SG-03 the centreline strain gauge was offset by 25mm to avoid this area. SG-03 gave more comparable centreline strain results to the DIC results; however, the furthest strain gauges had a large knot in the immediate vicinity (Fig. 10c and 10f) which impacted the strain distribution. Similar to the maximum tensile strain results discrete strain gauges tended to be less reliable at accurately capturing the full strain distribution across the entire CLT width due to local natural and manufactured imperfections in the wood material.

Results between the point load at centre and line load across the CLT panel width at midspan were comparable for the DIC and FEM. This indicated that any impact of the clinching effect of the steel loading beam across the width of the CLT on the EFW results was minimal.

6.3 – EFFECTIVE FLANGE WIDTH

The EFW for the CLT flange was evaluated using the FEM for each longitudinal layer as well as for the full flange depth (i.e., combined for both longitudinal layers). The EFW was largest for layer 3 due to the perpendicular middle layer acting to distribute the strains out to the extremities of the flanges. This is in line with the findings by Masoudnia et al. [8] who noted the properties of the perpendicular layer had a significant impact on the EFW. For the full-depth EFW, $b_{eff,FEM}$, the results were often very close to the individual layer 3 EFW. This was largely because layer 1 was close to the neutral axis of the T-beams and had much lower average strains than layer 3. Minimal deviations were observed between the results of the individual specimen models indicating a nominal influence of the changes in longitudinal MOE. The largest influence of the changing MOE occurred in layer 1 due to the percentage of tension and compression strain being significantly impacted by the ratio of CLT to glulam stiffness.

As shown in Table 3, the results of the estimated EFW from the proposed Eurocode 5 [11] equation for a midspan point load, $b_{eff,EC5}$, was 21% of the full CLT width, while the average EFW observed in the FEM was

significantly larger at 93% of the full CLT width. Although the DIC results were slightly less than the FEM results for the top edge strain distribution, the experimental EFW was also likely larger than the predicted $b_{eff,EC5}$. Overall, this indicated that (2) may be overly conservative for CLT-glulam T-beams with semi-rigid shear connections.

7 – CONCLUSION

The results of an experimental study on the strain behaviour in the CLT flange of MTC T-beams and how this compared to a validated FEM were presented herein. DIC was utilized to capture a large strain field across the full width of the CLT top surface and compared to discrete strain gauge data. DIC proved to be a valuable measurement technique for evaluating the EFW of experimental specimens as strain peaks and valleys due to local wood characteristics that can affect the strain readings of discrete strain gauges. The EFW determined using the DIC strain distribution was on average 89% for the point load configuration and 88% for the line load configuration. This compared well to the FEM results which were on average 94% for the point load and 93% for the line load. Discrepancies between the results are hypothesized to be attributed to the edge-gluing between longitudinal boards which is not currently captured in the FEM. Edge-gluing is expected to have a significant impact on the EFW but is not currently quantified in proposed design codes or current literature. The maximum compression stress tended to be overestimated by DIC by 17% when compared to the FEM results.

A modified method was proposed for the evaluation of the full-depth EFW of CLT flanges, which consist of multiple layers, to include the effects of rolling shear in perpendicular layers, and potential tensile strains in the lower layers. When applied to the T-beam evaluated herein, the full-depth EFW was largely dependent on the EFW of layer 3 due to layer 1 being close to the neutral axis and having much lower average strains. Further application of the proposed modified method should be conducted to evaluate its applicability for additional MTC configurations (e.g., cassettes, 5-ply flanges), and its capabilities of accurately capturing experimental behaviour.

The proposed Eurocode 5 [11] equation for the EFW when subjected to a midspan point load tended to substantially underestimate the EFW when compared to the FEM and experimental results. This equation may be overly conservative for CLT-glulam T-beams with semi-rigid shear connections and should be studied further.

ACKNOWLEDGEMENTS

This work was supported by the Natural Science & Engineering Research Council, Mitacs Accelerate, and Element5. In-kind donation of the self-tapping screws was provided by Rothoblaas. No involvement from the above funding sources were provided in the research and preparation of this article.

REFERENCES

- [1] Timoshenko S. *Strength of Materials - Part II Advanced Theory and Problems*. 3rd ed. New York - Toronto - London: D. Van Nostrand Company Inc.; 1956.
- [2] CSA. *CSA-O86-24 Engineering Design in Wood*. Toronto, Canada: 2024.
- [3] Foschi RO. *Rolling shear failure of plywood in structural components*. Vancouver, BC: 1970.
- [4] Davalos JF, Salim HA. Effective Flange Width for Stress-Laminated T-System Timber Bridges. *Journal of Structural Engineering* 1993;119:938–53. [https://doi.org/10.1061/\(ASCE\)0733-9445\(1993\)119:3\(938\)](https://doi.org/10.1061/(ASCE)0733-9445(1993)119:3(938)).
- [5] Apple DA, Woodward C. *Stress-Laminated / Steel T-Beam Bridge System*. 1996.
- [6] Bogensperger T. *Darstellung und praxistaugliche Aufbereitung für die Ermittlung mitwirkender Plattenbreiten von BSP-Elementen* 2013.
- [7] Thiel A, Augustin M, Bogensperger T, Schickhofer G. *Mitwirkende Breite bei Plattenbalken aus BSH und BSP - Kurzfassung und Anwendungsbeispiele* 2014.
- [8] Masoudnia R, Hashemi A, Quenneville P. Predicting the Effective Flange Width of a CLT Slab in Timber Composite Beams. *Journal of Structural Engineering* 2018;144:4018084. [https://doi.org/10.1061/\(asce\)st.1943-541x.0001979](https://doi.org/10.1061/(asce)st.1943-541x.0001979).
- [9] Dassault Systemes Simula Corp. *ABAQUS [Computer software]* 2020.
- [10] Hull T, Lacroix D. Parametric analysis of the effective flange width of mass timber composite floor panels. *Eng Struct* 2023;291:116370. <https://doi.org/https://doi.org/10.1016/j.engstruct.2023.116370>.
- [11] European Committee for Standardization (CEN). *Draft Eurocode 5: prEN1995-1-1*. Brussels: n.d.
- [12] Augustin M, Thiel A. *Proposal for the determination of the effective width and the verification of ribbed plates*. 2017.
- [13] European Committee for Standardization (CEN). *EN 1995-1-1:2004/A2:2014 – Eurocode 5 – Design of timber structures – Part 1-1: General – Common Rules and Rules for Buildings*. Brussels, Belgium: 2014.
- [14] Kleinhenz M, Viertel M, Demschner T, Frangi A. Determination of The Effective Width of Cross-Laminated Timber Rib Panels Using Digital Image Correlation. *13th World Conference on Timber Engineering, WCTE 2023* 2023;4:2416–25. <https://doi.org/10.52202/069179-0319>.
- [15] Chiewanichakorn M, Aref AJ, Chen SS, Ahn I-S. Effective Flange Width Definition for Steel–Concrete Composite Bridge Girder. *Journal of Structural Engineering* 2004;130. [https://doi.org/10.1061/\(asce\)0733-9445\(2004\)130:12\(2016\)](https://doi.org/10.1061/(asce)0733-9445(2004)130:12(2016)).
- [16] Hull T, Ackerman P, Lacroix D. Development of a glue bonded shear connections aimed for mass timber composites. *International Wood Products Journal* 2024;20426445241284950. <https://doi.org/10.1177/20426445241284954>.
- [17] ASTM. *Test Methods of Static Tests of Lumber in Structural Sizes D198-22a* 2022. <https://doi.org/10.1520/D0198-22A>.
- [18] Schreier H, Orteu JJ, Sutton MA. *Image correlation for shape, motion and deformation measurements: Basic concepts, theory and applications*. Springer US; 2009. <https://doi.org/10.1007/978-0-387-78747-3>.
- [19] Bigger R, Blaysat B, Boo C, Grewer M, Hu J, Jones A, et al. *A Good Practices Guide for Digital Image Correlation*. 2018. <https://doi.org/10.32720/idics/gpg.ed1/print.format>.
- [20] Correlated Solutions Inc. *VIC-3D Digital Image Correlation* 2024.
- [21] Hull T, Lacroix D. *Experimental Evaluation of Mass Timber Composite Panel Connections: Screw-Glued, Glue Pressed, and SHARP Metal Plates*. Submitted to: *Engineering Structures* 2025.
- [22] Bartolucci B, Rosa A, Bertolin C, Berto F, Penta F, Siani A, et al. Mechanical properties of the most common European woods: a literature review. *Fracture and Structural Integrity* 2020;14:249–74. <https://doi.org/10.3221/IGF-ESIS.54.18>.